# Journal Pre-proof

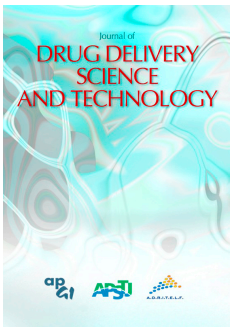


3D printed composite dressings loaded with human epidermal growth factor for potential chronic wound healing applications

Joshua Siaw Boateng, Forough Hafezi, Atabak Ghanizadeh Tabriz, Dennis Douroumis

PII: S1773-2247(23)00536-1

DOI: https://doi.org/10.1016/j.jddst.2023.104684

Reference: JDDST 104684

To appear in: *Journal of Drug Delivery Science and Technology*

Received Date: 2 April 2023

Revised Date: 3 June 2023

Accepted Date: 13 June 2023

Please cite this article as: J.S. Boateng, F. Hafezi, A.G. Tabriz, D. Douroumis, 3D printed composite dressings loaded with human epidermal growth factor for potential chronic wound healing applications, *Journal of Drug Delivery Science and Technology* (2023), doi: https://doi.org/10.1016/j.jddst.2023.104684.

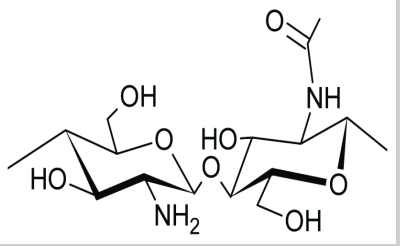


Chitosan

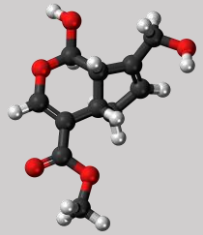

Genipin

Growth Factor

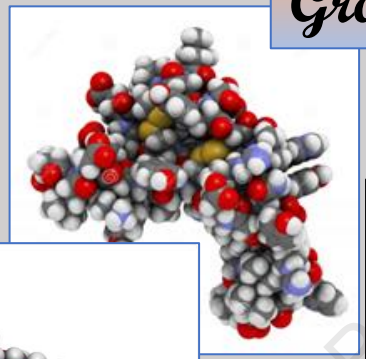

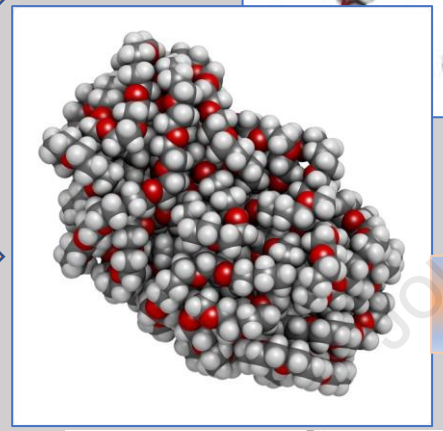

PEG

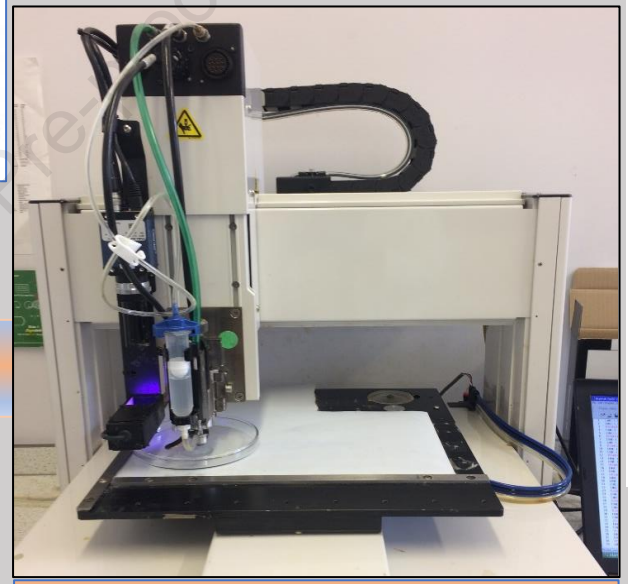

3D PRINTING

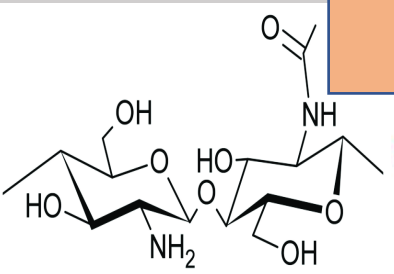


Chitosan

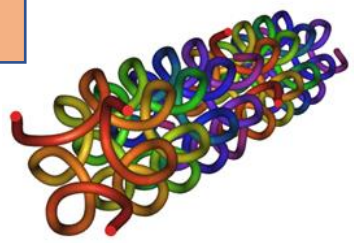

Collagen

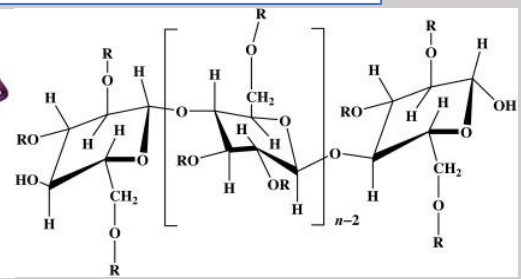


HPMC

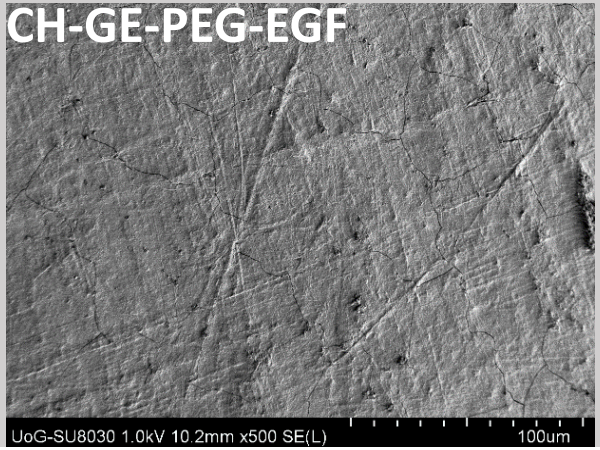


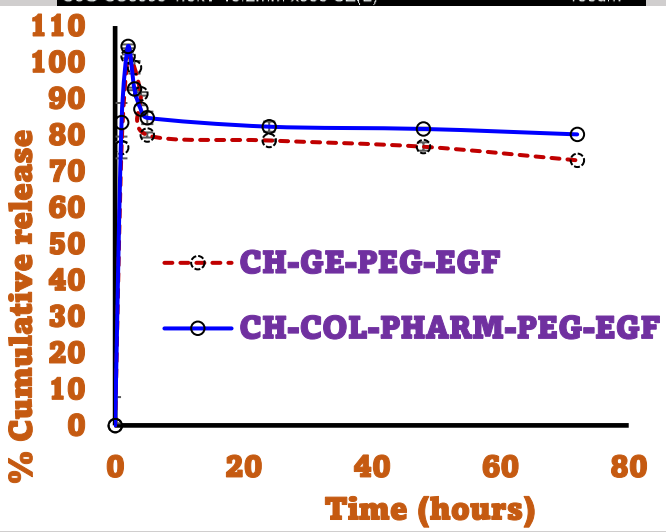


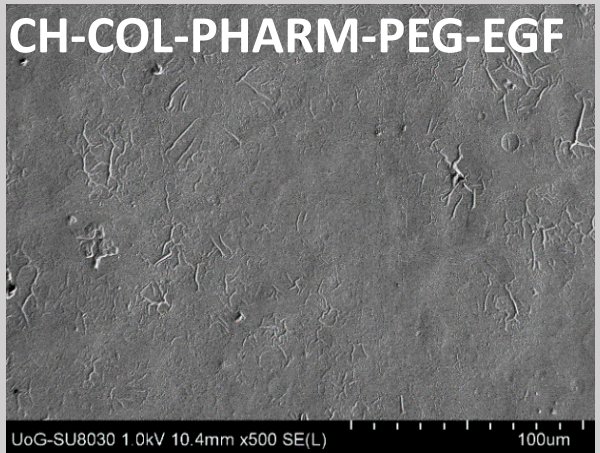

# 3D Printed Composite Dressings Loaded With Human Epidermal Growth Factor For Potential Chronic Wound Healing Applications

Joshua Siaw Boateng[1]*, Forough Hafezi[1], Atabak Ghanizadeh Tabriz[1], Dennis Douroumis[1]

[1] School of Science, Faculty of Engineering and Science, University of Greenwich, Medway, Central Avenue, Chatham Maritime, Kent, UK, ME4 4TB.

* Correspondence: j.s.boateng@gre.ac.uk

**Abstract:** This study formulated and characterized functional properties of 3D printed composite polymer-based film dressings comprising chitosan (CH) crosslinked with genipin (GE) or CH combined with collagen (COL) and loaded with epidermal growth factor (EGF). The films were characterized using texture analyzer (tensile, adhesion), swelling capacity, X-ray diffraction-XRD, Fourier transform infrared (FTIR) spectroscopy, scanning electron microscopy-SEM, drug dissolution, and MTT assay using human dermal fibroblasts. FTIR confirmed crosslinking between CH and GE, CH and COL as well as between CH and EGF while XRD showed amorphous matrix of the films. Mucoadhesion studies showed the films' ability to adhere to a model simulated wound surface. SEM demonstrated a smooth, homogenous surface indicating content uniformity. The swelling was higher for CH-GE than the CH-COL films while blank films swelled better than the EGF loaded films. EGF was initially released rapidly, reaching 100% in 2 h, subsequent sharp reduction till 5 h followed by sustained release till 72 h, while MTT assay showed greater than 90% cell viability after 48 h, confirming their biocompatibility. EGF loaded films showed higher cell proliferation than blank equivalents. Overall, the results showed the potential of CH based 3D printed films as suitable dressing platforms to deliver EGF directly to chronic wounds.

**Keywords:** 3D printing; chitosan; collagen; epidermal growth factor; films; wound healing.

## 1. Introduction

Wound healing comprises a complicated set of interrelated biochemical and molecular events including the clotting cascade, inflammation, synthesis and deposition of collagen, formation of new blood vessels, fibroplasia, epithelialization, and formation of cellular connective tissue [1]. The clot from the coagulation phase initially secretes various cytokines and growth factors such as platelet derived growth factor and epidermal growth factor (EGF) that stimulate the tissue regeneration process [2,3]. Lots of other growth factors are involved in the different phases of wound healing, therefore various authors have proposed their direct application to chronic wounds to enhance the wound healing process [4,5].

EGF is a peptide composed of 53 amino acids and was originally isolated from mouse submaxillary gland [6] with four proteins comprising the EGF family including EGF, transforming growth factor alpha (TGF-α), heparin-binding EGF and amphiregulin, [4]. EGF functions by facilitating the regeneration of epidermal cells and is very important in dermal wound healing by stimulating keratinocyte proliferation and migration [7] while also stimulating granulation tissue formation and motility of fibroblast cells.

One of the major challenges with administration of growth factors is their low stability and development of formulations designed to stabilize and enhance peptide function, have resulted in a resurgence in their use for wound healing purposes [5,8]. Such platforms overcome some of the side effects encountered at non-target sites when administered via injections and directly target the wounded site by using polymer macromolecules. This could provide growth factor-based therapies that can target the molecular biochemical processes occurring within chronic wounds, which are typically stuck in an inflammatory cycle and thereby stimulate healing [4].

Various dressings such as sponges and films have been explored for delivering drugs to wound sites [9]. Film dressings are elastic and flexible, and inspection of wound healing progression is also possible without the need to remove the wound dressing because of their transparent nature.

Chitosan (CH) based matrices have been employed in tissue engineered scaffolds such as cartilage, and skin due to its excellent biomedical characteristics such as biocompatibility, biodegradability, bioadhesion and low antigenicity [10]. In addition, CH is widely formulated with other polymers, including hyaluronic acid, poly (3-caprolactone), and poly (l-lactic acid) for tissue engineering applications. Collagen (COL) is the most abundant protein in the human body by mass, providing the building blocks for tissues such as bones, tendons, dermis, and corneas [11]. In previous studies, CH and COL have been combined in

composite matrices for tissue regeneration [12]. CH caused the matrices to exhibit better mechanical properties with reduced matrix erosion while COL improved the matrices' cell affinity and resulted in a lower degradation rate and higher mechanical strength, with COL significantly helped to optimize cellular affinity of the dressing [13]. Afzali and co, reported on COL based composite dressings for wound healing applications [14] and showed that the weak mechanical properties of COL required the presence of other stabilizing polymers such as sodium alginate to improve the physical and mechanical stability.

Matrices such as film-based dressings have traditionally been formulated using formulation technologies such as hot melt extrusion, solvent casting, and spray coating which have the advantage of being easy to prepare and relatively cheap [15]. However, these techniques have various disadvantages at the micro level including inability to precisely control important performance characteristics such as the microarchitecture and pore geometry. These significantly affect ideal properties such as exudate handling and control, bioadhesion and drug release mechanisms [16]. 3D printing methods produce well organized structures from a 3D design file, and the required shape is then fabricated by depositing layer upon layer and building up the structure one step at a time. This allows better control of the microstructure and geometric architecture which significantly affects other important characteristics that impact on their performance *in vivo*, such as exudate handling and drug release. 3D printing has the ability to predetermine and control such performance characteristics in addition to more advanced possibilities such as depositing chemical or biochemical sensors into the printed matrix [17] as well as embedding cells through bioprinting approach [18].

Therefore, this study aimed to develop medicated 3D printed composite CH based film matrices comprising CH crosslinked with GE or CH physically mixed with COL, optimize physical and chemical properties and ultimately loading with EGF as a model growth factor to stimulate healing of hard to heal wounds. The formulations have been characterized for chemical and physical (SEM, XRD, FTIR, mucoadhesion, swelling) properties, release of EGF and MTT assay to determine cell viability as indicator of biocompatibility and the cell's ability to proliferate in the presence of the EGF loaded films.

## 2. Materials and Methods

### 2.1 Materials

Chitosan (low molecular weight, degree of deacetylation = 75-85%), dimethyl sulfoxide (DMSO), gelatin, fetal bovine serum, potassium dihydrogen phosphate buffered saline, were obtained from Sigma Aldrich (Gillingham, UK). MTT (3-(4, 5-dimethylthiazol-2-yl)-2, 5-diphenyltetrazolium bromide), glycerol, penicillin/streptomycin solution, potassium chloride, sodium phosphate dibasic, sodium hydroxide, acetic acid and polyethylene glycol (200-600) were obtained from Fisher Scientific, (Loughborough, UK). Dermal cell basal medium, Dulbecco's Modified Eagle's Medium (DMEM), human dermal fibroblast (HDF) and trypsin EDTA solution for primary cells were obtained from ATCC, Manassas, Virginia, USA. HPMC (Pharmacoat 603®-PHARM) was freely donated by Shin-Etsu Chemical Co., Ltd. (Tokyo, Japan). Epidermal growth factor was purchased from Alomone Labs Ltd. Jerusalem, Israel. Collagen type 1 was obtained from Shaanxi Guanjie Technology, (Shanghai, China). Genipin (GE) was obtained from Linchuan Zhixin Biotechnology Co., Ltd., Linchuan.

### 2.2 Methods

#### 2.2.1 Gel formulation and 3D printing

Preliminary formulation development was performed initially to determine optimum gel concentrations for blank formulations prior to growth factor loading and shown in Table 1 for the CH-COL based films while that for CH-GE based films have been previously reported [19]. EGF was loaded into optimized composite CH-GE and CH-COL based gels with optimum viscosities prior to printing. EGF loaded CH-GE films were prepared by initially adding CH (1.2 w/v) and PEG (plasticizer) to 0.5% v/v acetic acid with constant stirring, until a uniform gel was obtained. The resulting gel was covered and left to stand till all generated air bubbles disappeared. Afterwards, the combined gel solution of CH and PEG was added to EGF (0.1% w/v) and the crosslinker (GE, 1% w/v, 5 ml) added with constant stirring for another 30 min to ensure that the crosslinking of CH by GE was complete. The resulting homogeneous gel was poured into the syringe of a jet dispenser (583 Dispenser, Nordson-Asymtek, Maastricht, Netherlands) and printed onto a Petri dish and placed in an oven (30 °C) over 24 h to dry. The EGF loaded CH-COL based printed films were prepared by dissolving CH powder (1% w/v) and plasticizer (PEG) in 0.5% v/v acetic acid at room temperature. The resulting gel was then mixed with 1 % COL (w/v) with continuous stirring (5 min). Finally, PHARM (1% w/v) and EGF (0.1% w/v) were then added to the blend and the resulting gel was printed and dried as above. The difference in concentration of CH

between the two optimized formulations (1.2% in CH-GE films vs 1% in CH-COL films) was due to the fact that the final gel concentration chosen was determined by how closely their viscosity profiles matched the standard 3D printer bioink supplied by the instrument manufacturer.

Table 1 Different compositions of the starting materials (varying amounts based on total solid weight) used for formulating 3D printed CH-COL-PHARM films.

| Formulation | CH (g) | COL (g) | PHARM (g) | PEG (g) | GLY (g) | Total weight (g) | % GLY content | % PEG content |
|---|---|---|---|---|---|---|---|---|
| CH-COL-PHARM (A) | 0.30 | 0.20 | 0.15 | 0.00 | 0.00 | 0.65 | 0.00 | 0.00 |
| CH-COL-PHARM (B) | 0.40 | 0.10 | 0.15 | 0.00 | 0.00 | 0.65 | 0.00 | 0.00 |
| CH-COL-PHARM-PEG (C) | 0.30 | 0.20 | 0.15 | 0.10 | 0.00 | 0.75 | 0.00 | 13.33 |
| CH-COL-PHARM-PEG (D) | 0.30 | 0.20 | 0.10 | 0.15 | 0.00 | 0.75 | 0.00 | 20.00 |
| CH-COL-PHARM-GLY (E) | 0.30 | 0.20 | 0.15 | 0.00 | 0.10 | 0.75 | 13.33 | 0.00 |
| CH-COL-PHARM-GLY (F) | 0.30 | 0.20 | 0.10 | 0.00 | 0.15 | 0.75 | 20.00 | 0.00 |

### 2.2.2 Weight, thickness and folding endurance

The weight and thickness of each film were examined as part of the physical characterization of the formulations. The thickness of the films was measured with the help of Vernier dial caliper gauge micrometer screw, by placing the gauge at three random corners of the original film. The flexibility of CH-COL-PHARM 3D printed films having different concentrations of PEG or GLY was evaluated by continuously folding the 3D printed film at an angle of 180° to the horizontal plane at the same position till the film broke or 300 folds with no evidence of break or tear in the film.

### 2.2.3 Tensile properties

Tensile behavior of the 3D printed films was evaluated with a texture analyzer (HD plus, Stable Micro System, Surrey, UK) fitted with a 5 kg load cell. Samples were cut into dumbbell shaped strips with the following dimensions: 80 mm in length, gauge length and width of 30 and 3 mm respectively. The cut strips ($n$ = 3) were stretched (2 mm/s) between the tensile grips until they broke, using with a low trigger force (0.049 N). Tensile strength (peak force per unit area), the elongation at break (%), elastic modulus (gradient of force-distance curve) and work done to break the films (area under the force-distance curve) were calculated using appropriate equations [20,21].

### 2.2.4 X-ray diffraction (XRD)

The physical form of pure polymers (CH, COL and PHARM), plasticizers (GLY, PEG) and 3D printed films was analyzed using an X-ray diffractometer (Bruker AXS GmbH, Karlsure, Germany). For pure powders, Mylar was employed to hold the samples together before being placed on the sample cell. The films were cut into small pieces, arranged on top of each other in a holder and eventually placed in the sample cell. The samples were analyzed in transmission mode using the following settings (diffraction angles 5° to 50° 2θ, step size 0.04°, scan speed 0.4 s/step).

### 2.2.5 Fourier transform infrared (FTIR) spectroscopy

The starting materials and 3D printed films were analyzed on an attenuated total reflectance (ATR) FTIR spectrophotometer (Perkin Elmer Vatrtwo, Massachusetts, USA) equipped with OMINC® software from 4000–450 $cm^{-1}$ with an average of 64 scans. Small cut pieces of film were placed on the ATR diamond crystal and a pressure clamp used to apply force for proper contact. In the case of starting materials, a small amount of powder was placed on the diamond crystal and the analysis performed in the same way as the films. Prior to the analyses, background spectra were captured and this was subtracted from each sample's spectra to ensure consistent results.

### 2.2.6 Scanning electron microscopy (SEM)

The 3D printed films were evaluated for their surface architecture and geometry on a Hitachi SU 8030 scanning electron microscope (Hitachi High Technologies, Krefeld, Germany). Cut samples were applied onto aluminium pin-type stubs, using carbon tapes that were adhesive on both sides, sputter-coated with chromium (Edwards 188 Sputter Coater S1508) and

analysis performed using accelerating voltage of 1 kV. Images were obtained by *i-scan* 2000 software at different magnifications (x40 – x5000).

### 2.2.7 Mucoadhesion studies

The adhesive behavior of the printed films was investigated using the texture analyzer described above with set gelatin (GEL), prepared from 6.67% w/v of GEL solution, 60 °C) and placed in a fridge to solidify. Prior to the mucoadhesion test, PBS (500 µL, pH 7.4 ± 0.1) [22] was spread in the surface of the GEL to represent an exuding wound surface. Circular strips of film with same diameter as the adhesive probe were stuck to the probe (35 mm) and brought in contact with the GEL surface for 60s. The film in contact with the simulated wound surface (GEL) was detached at a speed of 0.5 mm/s using a trigger force of 0.05N. The following adhesive properties –peak adhesive force, cohesiveness and total work of adhesion (TWA), were determined using the force distance plots with the help of the Texture Exponent 32 software.

### 2.2.8 Water (exudate) handling

The swelling index (swelling capacity) of the 3D printed films was assessed as previously reported [23] using the PBS prepared above (pH 7.4 ± 0.1, 37 ± 0.1 °C) as a measure of exudate handling ability. Accurately weighed film strips ($n$ = 3) were placed in 5 ml of PBS and the change in weight with time recorded up to 120 min. This involved removing the swollen film from PBS at each time interval, blotted with filter paper and then weighed instantly. Equation 1 was used to calculate the percent swelling index (or swelling capacity) Is (%).

$$Is = \frac{Ws - Wd}{Wd} \times 100 \quad (1)$$

Where $W_d$ is the dry weight of the films and $W_s$ is the weight of film after swelling.

### 2.2.9 *In vitro* drug dissolution studies

Before the dissolution studies, EGF content within the CH-GE-PEG and CH-COL-PHARM-PEG films was analyzed. The accurately weighed (25 mg) 3D printed films containing EGF ($n$ = 3) was completely immersed acetic acid (10 ml of 0.5% (v/v)). The hydrated film was left to sonicate for 1 h followed by constant stirring on a magnetic stirrer to ensure the CH present in the films was completely dissolved. For the in vitro drug dissolution experiment, 10 ml of PBS (pH 7.4, 37 °C) as dissolution medium was placed in glass vials with

continuous stirring (200 rpm). PBS was used instead of simulated wound fluid because the presence of albumin in the latter tended to block the HPLC column and also interfered with detection of the model protein drug EGF. Previously weighed film samples (20 – 40 mg) were placed in the PBS and 1 ml aliquots removed are regular time intervals up to 48 h. To ensure constant volume of dissolution medium and maintain sink conditions, the sampled PBS was replaced with fresh dissolution medium at the same temperature. For both the EGF content assay and dissolution tests, the PBS was passed through filter cartridges into HPLC vials. The EGF concentration (assay and amount released at each time point) was analyzed on an Agilent 1200 HPLC system by injecting 20 µl of the filtered samples. The stationary phase used was a C18 Hichrom Kromasil column with particle size of 5 µm, column length and internal diameter of 250 mm and 4.6 mm respectively, while PBS was used as the mobile phase with flow rate and detection set at 1 ml/min and 214 nm respectively. The concentration of drug in each film (assay) and released at each time point (dissolution) was calculated using an EGF linear calibration curve (10 - 50 µg/ml, $R^2 > 0.99$)(LOD and LOQ were 12.5 and 37.8 µg/ml respectively).

**2.2.10 MTT assay (cell viability)**

To determine viability and proliferation potential and cytotoxicity of the EGF loaded films, MTT assay was performed using human dermal fibroblast cells (HDF) (ATCC®SCRC1041™). Before the analysis, each film sample was left to sterilize overnight in a UV flow cabinet (NU-437-300E, NUAIRE) after which they were placed in 96 well plates. Subsequently, 100 µl of cell suspension (1 x $10^5$ cells/ml) was dropped onto the films within the well plates and placed in an incubator at 37 °C in 5% (v/ v) $CO_2$ for up to 72 h to allow attachment of the cells to the wells. At 24, 48 and 72 h, aliquots (10 µl) of sterile MTT stock solution equivalent to50 µg of the pure compound, were added to the well plates containing samples (including negative and positive controls). The samples mixed with the MTT reagent were put back into the incubator for a minimum of 4 h till the appearance of a purple precipitate upon observation under an inverted microscope (AE2000, Motic). Once this was confirmed, all media was aspirated from the wells and replaced with DMSO (100 µl), placed in the incubator over a 30 min time period after which a plate reader (Multiskan FC, Thermo Scientific) was used to measure the absorbance (492 nm) in each well. Three technical replicates were performed and repeated three times per sample, therefore providing total of $n = 9$ replicates. The negative and positive controls employed were the HDF cells with no sample treatment and cells treated with 0.01% w/v Triton-X-100 respectively. The

results of the optimal cell density curve were normalized at logarithmic scale. Equation 2 was used to determine the cell viability.

$$\text{Percentage cell viability} = \frac{\text{At}-\text{Ab}}{\text{Ac}-\text{Ab}} \times 100 \quad (2)$$

$A_t$, = absorbance reading for test samples; $A_b$ = absorbance of medium only; $A_c$ = absorbance of untreated cells.

### 2.2.11 Statistical analysis

All the quantitative data for the different samples tested were compared using one-way analysis of variance (ANOVA) with significant difference set at $p \leq 0.05$.

## 3. Results and Discussion

### 3.1 Formulation development

The jet dispenser used in this research employed a pneumatic piston with a ball-tip at its end to direct the composite gels through a small orifice located on the jet nozzle as was previously described [24]. A 400 μm nozzle (Nordson, Deurne, Netherlands) was selected in this study as this allowed the viscous composite gels to be dispensed and printed in a highly reproducible and efficient way. For both CH-GE and CH-COL based films, there was a need for a plasticizer to reduce brittleness resulting in the production of more flexible films that did not break easily, and this was evaluated quantitatively as outlined in section 3.2.

### 3.2 Mechanical characteristics

The mechanical properties were evaluated by folding endurance as well as tensile strength, percentage elongation (flexibility), and Young's modulus (measure of the stiffness of the film).

### 3.2.1 Folding endurance

The folding endurance is used to determine ease of handling and is indicative of a film's brittleness or flexibility and therefore complemented the tensile characterization results discussed in section 3.2.2. Formulations showing folding endurance values of ≥ 300 are deemed to have ideal flexibility for easy handling without damage and easy to apply [25]. All the 3D printed films did not break after folding 300 times and this suggests the 3D printed films had acceptable flexibility. Takeuchi developed an automatic folding endurance method

compared with standard tensile testing approach on films prepared from hydroxypropylmethylcellulose (HPMC), polyvinyl alcohol and hydroxyproyl cellulose. The HPMC films were plasticized with different amounts of glycerol (5 – 30%). At lower plasticizer concentrations (5 – 10%), the folding endurance decreased and increased at higher plasticizer (20 – 30%) concentrations [26]. Khan and co-authors investigated the folding insurance of CH films and their results demonstrated that formulation variables such as concentrations of CH, plasticizer and crosslinker had a significant impact on the mechanical characteristics of films [27]. Folding endurance by manual bending provides a quick indication of film flexibility and depicts potential for easy handling during application. However, it does not provide a quantitative measure of the film's strength and toughness and therefore texture analysis was performed to measure the films' tensile properties.

### 3.2.2 Tensile properties

The tensile characteristics for blank CH-COL 3D printed films plasticized with either GLY or PEG are shown in Figure 1a, while those of CH-GE films were previously reported [19]. Both formulations showed similar tensile behavior with changing plasticizer concentrations. The 3D printed CH-COL-PHARM-GLY (E) films with 13.33 % w/w of GLY exhibited relatively low value for percent elongation at break (16.71%) and high elastic modulus (13.56 N/mm). This is indicative of a brittle film which will not be appropriate for applying onto a healing wound due to risk of damaging newly formed skin cells/tissues. The CH-COL-PHARM-PEG (D) and CH-COL-PHARM-GLY (F) films, plasticized with 20% w/w of GLY or PEG, both exhibited percentage elongation at break value of 82.62%, which were deemed too high, while exhibiting very low tensile strength values of 4.65 and 2.54 $N/mm^2$ respectively. Different researchers [28,29] studied the relationship between elastic modulus and elongation in films and showed that films with high percentage elongation showed lower values for elastic modulus and tensile strength.

The addition of a plasticizer can overcome brittleness and film rigidity by interrupting the polymer chain interactions. However, too much plasticizer can decrease the adhesivity of films by overhydrating the formulations [30] and can make the final product sticky and difficult to handle and apply. Furthermore, such high amounts of plasticizer and subsequent overhydration can cause excess exudate to be accumulated underneath the dressing with a resultant risk of maceration of surrounding healthy skin. Consequently, this could result in further complications including infections with potential for the wound to become chronic [31,32]. CH-COL-PHARM-PEG (C) films containing 13.33% w/w of PEG200 showed

314 percentage elongation at break of 26.23% and CH-GE films obtained from 1.2% w/v CH gels
315 and plasticized with PEG600 at CH:PEG ratio of 1:1 showed elongation at break of 22.67%.
316 Therefore, based on ASTM standards for thin films, percentage elongation at break values of
317 20-50%, these two films were within the acceptable range (ASTM, 2015) and were selected
318 as the optimum formulation for EGF loading. In general, low molecular weight plasticizers
319 can facilitate better plasticizer–polymer molecular chain interactions [33]. However, our
320 results showed that GLY (92.09 g/mol) plasticized the films more extensively in comparison
321 to PEG. Compared to the CH-GE films, the CH-COL based films showed significantly ($p <$
322 0.05) weaker films with lower overall tensile strength and elastic modulus values.
323 Figure 1b shows the tensile profiles of the EGF loaded . The average tensile strength
324 (27.14 N/mm$^2$) and % elongation (24.59%) of EGF loaded CH-GE-PEG films was not
325 significantly different from the tensile strength (30.24 N/mm$^2$) and % elongation (22.67%) of
326 blank films which could be attributed to the relatively low quantities of EGF present in the
327 drug loaded formulations. The tensile strength (15.98 N/mm$^2$) of EGF loaded CH-COL-
328 PHARM-PEG films was significantly ($p < 0.05$) higher than tensile strength (9.12 N/mm$^2$) of
329 blank CH-COL-PHARM-PEG 3D printed films shown in Figure 1a. Hong and co-authors
330 investigated the impact of exogenously administered EGF on diabetic foot ulcers and found
331 that the EGF-loaded dressings showed an increase in their tensile strength and direct
332 application of EGF embedded within advanced dressing could have great potential for
333 enhancing the healing of such chronic ulcers [34]. Both 3D printed CH-GE-PEG-EGF
334 (24.59%) and CH-COL-PHARM-PEG-EGF (27.21%) films showed acceptable values of %
335 elongation making them ideal dressings with ideal toughness which will allow handling and
336 flexibility for easy application. It also shows that the low amount EGF did not impact
337 negatively on the tensile behavior of both optimized composite formulations. Finally, elastic
338 modulus and tensile strength of CH-GE-PEG-EGF films was significantly ($p < 0.05$) higher
339 than the CH-COL-PHARM-PEG-EGF as observed in the blank films. This could be
340 attributed to the chemical crosslinking of CH by GE while the CH-COL based films only
341 involved physical mixing of the different components, therefore exhibiting weaker
342 mechanical strength.
343
344 **3.3 X-ray diffraction (XRD)**
345 Figures S1 and S2 (supplementary data) show the XRD patterns of the pure polymer powders
346 (CH, COL and PHARM) and blank 3D printed CH-COL-PHARM-PEG films respectively,
347 which all showed amorphous nature. Figure 2 shows the transmission diffractograms of EGF

loaded CH-GE-PEG and CH-COL-PHARM-PEG 3D printed films. Both diffractograms showed a broad peak between 20° and 25° and another peak at 9.8° [35]. This is in full agreement with the XRD diffractogram of pure CH and confirms that CH is the predominant polymer within the formulations. Liu and co-authors [36] investigated the structural characteristics of CH films and their results were comparable to that obtained for this study. They exhibited peaks at 10° and 20.5° which are characteristic of CH and showed similar intensity. According to the literature [37], EGF is a typical growth-stimulating peptide which is known to have a crystalline structure. However, no obvious crystallinity was observed in either EGF loaded films which indicates that both formulations were amorphous. This suggests the molecular dispersion of EGF within the matrix of the composite formulations and confirms the successful crosslinking between CH and GE.

### 3.4 Fourier transform infrared spectroscopy (FTIR)

Figures S3 and S4 show spectra of the pure materials and blank printed films. As shown in Figure S4 all 3D film printed films showed a band at 1653 $cm^{-1}$ which is due to acetyl amide I and another absorption band at 1586 $cm^{-1}$due to an amine group. Lu and colleagues [38] investigated the reactions in CH-COL films and reported comparable results where the addition of COL caused the amide I and amine bands of CH to shift. This implies hydrogen bond interactions between the CH and COL as reported by others [39]. The amide I band at 1653 $cm^{-1}$ decreased in intensity compared to the amide II peak at 1550 $cm^{-1}$ indicating interaction between CH's $–NH_2$ groups and the PEG chains [40]. The –OH, $–NH_2$ and –C=O groups in COL can form hydrogen bonds with –OH and $–NH_2$ groups of CH [41]. Furthermore, at acidic pH, the amino groups of CH are in the protonated form, which enables electrostatic interactions between $NH_3^+$ of CH and –COO present on aspartic and glutamic acid groups in COL. In addition, as the COL content in the films decreased, the intensity of the amide I band also decreased, eventually showing up only as a small shoulder next to the peak for the amide II functional group. These interactions made the 3D printed films exhibit better mechanical (tougher and more flexible) and handling properties.

Figure 3 shows the FTIR spectra of EGF loaded CH-GE-PEG and CH-COL-PHARM-PEG 3D printed films. Both spectra for the CH-GE-PEG-EGF and CH-COL-PHARM-PEG-EGF films showed peaks at 3439 $cm^{-1}$, which correspond to the stretching vibration of $–NH_2$ and –OH groups in CH, while the peak at 1657 $cm^{-1}$ was attributed to the $–CONH_2$ group, and another sharp peak at 1568 $cm^{-1}$ arising from $–NH_2$ bending vibration. The width of the peak at 3439 $cm^{-1}$ increased for both EGF loaded films compared with the

blank films and was attributed to further hydrogen bonding sites due to loading of the growth factor. This shows there was electrostatic interaction between EGF and CH. The peak at 1568 $cm^{-1}$ for the amino group in CH gets protonated to produce the ammonium ion, resulting in new bands at 1642 and 1547 $cm^{-1}$ in the EGF loaded films. The additional hydrogen contributed by EGF made the 3D printed films more rigid. As was demonstrated above (Figure 1) CH-COL-PHARM-PEG 3D printed films had a tensile strength of 9.12 $N/mm^2$, while CH-COL-PHARM-PEG-EGF films exhibited tensile strength of a 27.14 $N/mm^2$ which confirms the contribution of EGF in increasing the mechanical strength of the films. Rajama and co-authors [42] characterized CH nanoparticles incorporating EGF and fibroblast growth factor and demonstrated that the presence of EGF provided extra sites for hydrogen bonding resulting in more rigid nanocomposites.

### 3.5 Scanning electron microscopy (SEM)

SEM images of the optimized blank 3D printed CH-GE-PEG and CH-COL-PHARM-PEG films selected for EGF loading are shown in Figure 4a and the other formulations shown in Figure S5. The surface of the films was smooth and homogeneous with no pores apparent in the microstructure and shows good distribution of the starting materials within the composite formulations. The films with no or low amounts of plasticizer exhibited micro-cracking attributed to tight packing in the matrix architecture [36] and was in agreement with the tensile results which showed that unplasticized films exhibited brittleness.

Various authors have reported on the impact of naturally occurring plasticizers e.g. GLY and sorbitol on polysaccharide-based films [43,44]. Tarique and co-authors investigated the effect of GLY on the physical, mechanical, thermal and barrier properties of starch biopolymer based films and based on their results, films plasticized with GLY showed reduced brittleness, higher thermal stability and homogeneity and increased water vapor permeability [45]. Vieira and co-authors studied the effect of plasticizers on the plasticizing efficiency and stability during storage for CH based films and demonstrated that both GLY and PEG were better plasticizers compared to others that were tested. In addition, they showed that incorporation of 20% (w/v) of GLY or PEG into the starting gels resulted in CH films, that were stable over a 5-month period [46].

Figure 4b shows SEM images of CH-GE-PEG-EGF and CH-COL-PHARM-PEG-EGF 3D printed films. The surface of both films was continuous without visible surface pores indicating that all components exhibited good miscibility and compatibility. Little patches could be seen which are attributed to air bubbles that travelled from the mass of the film-

forming solution to the surface during drying. Sionkowska and co-authors reported the same morphological characteristics for CH/COL films [47,48]. Faikrua and co-authors demonstrated that scaffolds with non-porous microstructure had high tensile strength with resultant decrease in flexibility [49]. However, scaffolds are expected to have sufficient strength therefore their structural integrity is maintained during testing *in vivo* and in cell growth *in vitro*. Both CH-GE-PEG-EGF and CH-COL-PHARM-PEG-EGF 3D printed films showed little pores and a smooth surface which confirms the results obtained during mechanical testing.

### 3.6 Mucoadhesion

The adhesive results for the blank CH-GE films have been previously reported and the plasticized films showed a high detachment force of (3.05 ± 0.56 N) and TWA (1.986 ± 0.17 N.mm) compared to unplasticised films (CH-GE) [19]. Figure 5a shows adhesive profiles for blank CH-COL based films with formulation C showing a higher PAF (1.38 ± 0.05 N) and TWA (1.09 ± 0.2 N.mm) compared to (D), (E)and (F).

These observations can be explained by the effect of PEG which enhances adhesivity by providing more hydrogen bonding sites to interact with the gelatin simulated mucosal surface. This therefore improves the adhesive performance based on the diffusion theory of mucoadhesion [50, 51] . In addition, the presence of PEG allowed better hydration of the films which is an essential process in the first phase of adhesion as it enhances the ability of the film and gelatin polymeric chains to interpenetrate more effectively, with a resultant increase in the PAF. According to Tapia-Blácido and co, low molecular weight plasticizers allow better interaction with polymeric chains [52], however, their results showed that GLY (92.09 g/mol) CH-COL-PHARM films better compared to PEG200 (190 – 210 g/mol) which led to films with lower PAF, and this observation has been reported by other investigators [53,54]. However, in this study, the PEG plasticized films generally performed better than the corresponding GLY plasticized films and might be related to different grades of polymers and PEG employed.

Figure 5b shows the adhesive profiles for the CH-GE-PEG-EGF and CH-COL-PHARM-PEG-EGF formulations. Both EGF loaded CH-GE-PEG-EGF [PAF of (3.54 ± 0.07 N) and TWA (0.91 ± 0.1 N.mm)] and CH-COL-PHARM-PEG-EGF [PAF of (1.92 ± 0.07 N) and TWA (1.63 ± 0.1 N.mm)] 3D printed films showed a high PAF and TWA compared to the corresponding blank formulations. This could be attributed to the adhesive effect of EGF on the films. Ramineni and co-authors [55] investigated the adhesion properties of EGF on

mucoadhesive films in humans and showed that EGF loaded films exhibited higher PAF to the oral mucosa for up to 4 h compared to the films without EGF. On the other hand, comparing EGF loaded 3D printed films showed that CH-GE-PEG-EGF had a significantly higher PAF and TWA than the CH-COL-PHARM-PEG-EGF.

These results can be explained by the concentration as well as molecular weight of CH and PEG (plasticizer) in each film as CH-GE-PEG contained 1.2% w/v CH and PEG600, whereas CH-COL-PHARM-PEG contained 1% w/v CH and PEG200. Generally, polymers that possess hydroxyl, amine and carboxyl, functional groups have potential to increase the residence time of formulations such as films on moist surfaces [56]. The mucoadhesive property of CH is due to various molecular forces of attraction, primarily hydrogen bond interactions between CH and the -OH and - $NH_2$ groups present in mucin which is a glycoprotein. Another characteristic of CH that contributes to its mucoadhesive performance is the conformational flexibility of its linear chain. The reactive primary amine groups of CH help in the formation of different molecular interactions (intra- and inter) which enhances cohesion/adhesivity between the CH film and the GEL (model wound substrate) [57]. Furthermore, polymers with low molecular weight are able to interpenetrate better while those with higher molecular weights show better entanglement. CH films containing propranolol hydrochloride, triethyl citrate and plasticized with PEG were three times more mucoadhesive than their corresponding unplasticized films [58].

### 3.7 Water (exudate) handling

Swelling experiments were undertaken to determine the printed scaffolds' ability to effectively absorb and handle wound exudate, using PBS at pH 7.4 to represent wound exudate [23]. This test is gravimetric and measures the maximum percentage weight of fluid absorbed and retained by the films [59] and is indicative of how effectively a dressing will perform under highly exuding chronic wound extreme conditions.

The swelling behavior of CH-COL-PHARM-PEG based 3D printed films is shown in Figure 6a. The formulations containing 13.33% PEG [CH-COL-PHARM-PEG (C)] had the maximum swelling capacity of 635 ± 65 % and followed by films containing 20% PEG [CH-COL-PHARM-PEG (D)] with a swelling capacity of 481 ± 65%. 3D printed films containing 20% GLY [CH-COL-PHARM-GLY (F)] had a lower swelling capacity of 402 ± 42% and followed by films containing 13.33% GLY [CH-COL-PHARM-GLY (E)] with a swelling capacity of 374 ± 27%. Compared to the CH-GE films [19], the swelling capacity of the CH-COL based films were significantly lower ($p < 0.05$), which is attributed to higher amounts of

CH in the former as well as the crosslinking by GE which afforded it hydrogel properties that enable it to absorb and retain. The swelling capacity for all the printed films increased in the first 5 min but the swollen films maintained their structural integrity. However, by 40 min the films became fully hydrated and reached maximum swelling and the swelling capacity decreased gradually (likely due to breaking apart of small fragments) for all films until 80 - 90 min when the swell reached a steady state. Further, the 3D printed films plasticized with PEG showed higher swelling capacity than films plasticized with GLY. Plasticizers generally work by increasing the intermolecular spaces between the polymer chains, which allows easier ingress with resultant increase in hydration rates, and this subsequently causes higher swelling capacity [60].

The swelling behavior of the CH-GE-PEG-EGF and CH-COL-PHARM-PEG-EGF films is shown in Figure 6b. The EGF loaded films had lower swelling index than the corresponding blank films due to the stronger mechanical strength from the tensile data above. The CH-COL-PHARM-PEG-EGF films showed a maximum value of 268 ± 40% but the CH-GE-PEG-EGF films showed value of 238 ± 43%. The swelling for both EGF loaded film formulations increased rapidly in the first 5 min but started losing their structural integrity around 60 min, followed by a gradual decrease in swelling till a steady state was achieved at 100 min.

Though the CH-GE-PEG-EGF films had lower maximum swelling capacity than the CH-COL-PHARM-PEG-EGF films, they showed higher swelling index values and sustained their swollen structure better over the 120 min testing period and this could be attributed to the crosslinking with GE. However, the difference in swelling capacity between CH-GE-PEG-EGF and CH-COL-PHARM-PEG-EGF 3D printed films was not significant ($p > 0.05$). Based on the studies of other researchers [61] the more amine groups in CH hydrogels are crosslinked, the more CH forms a more compact structure. In addition, the strength of polymer hydrogel was affected by the amount of added crosslinking agent [62]. Cassimjee and co-authors [63] investigated the performance of GE-crosslinked CH and hyaluronic acid matrices for neural tissue engineering applications and demonstrated that the matrices crosslinked with GE, showed improved swelling and greater resistance to degradation in PBS media at pH 7.4.

### 3.8 *In vitro* drug dissolution studies

The calibration graph using PBS as dissolution media is shown in Figure S6 showing the linear relationship between concentration and absorbance. The drug release profiles in PBS

for the CH-GE-PEG-EGF and CH-COL-PHARM-PEG-EGF 3D printed films are shown in Figure 7. A burst effect occurred initially, after which EGF was released over a longer time period at a slower rate. Almost 76% and 83% release of EGF was achieved within the first hour for CH-GE-PEG-EGF and CH-COL-PHARM-PEG-EGF respectively. The percentage release increased for both films and reached 100% in 2 h and decreased sharply between 3 and 5 h. Subsequently, the amount released decreased only slightly from 5 to 24 h for both films. Alemdaroglu and co-workers [64] investigated the release profiles of CH gels containing EGF for wound healing applications and their results also indicated that the release of EGF from the CH gel was 97% after 24 h. The percentage release decreased further to 80% for CH-COL-PHARM-PEG and 73% for CH-GE-PEG at 72 h suggesting possible EGF degradation in the dissolution medium with time. Therefore, EGF loaded dosage forms typically require high initial doses and/or regular administrations which presents risks of potential side effects such as cancer, while also increasing treatment costs [65]. More advanced delivery platforms with the ability to maintain the stability of loaded growth factors while controlling their release into the wound (e.g., nanoparticle encapsulation), can provide more effective and safe treatment options [5, 66].

The *in vitro* drug dissolution profiles mirrored the swelling results, with the films showing rapid hydration in the first 15 min resulting in rapid release, within 1 h. This indicates swelling dependent drug release which allows dissolution and release of the EGF from the swollen matrix as well as erosion of the matrix into the dissolution medium. In an ideal medicated dressing, drug release over 24 h or longer will be convenient for patients by avoiding frequent dressing changes. Figure 7 shows that for CH-COL-PHARM-PEG-EGF and CH-GE-PEG-EGF about 76% (67 µg) and 56% (50 µg) of the growth factor remained after 48 h which indicates that there might be no need for the dressing to be changed daily. However, other factors such as type, size and depth of wound, and the exudate produced [67, 68] determine the frequency of dressing changes. The difference between the mean % release for EGF loaded CH-GE-PEG and CH-COL-PHARM-PEG 3D printed films was not significant ($p > 0.05$).

### 3.9 MTT assay (cell viability)

Figure S7 shows the cell viability data from MTT assay of the blank CH-COL-PHARM-PEG and CH-COL-PHARM-GLY based formulations while that for the blank CH-GE-PEG films was previously reported [19]. The results demonstrated that the cell viability

for all the blank CH based 3D printed films remained above 90% after 24 and 48 h of incubation which shows their biocompatibility with HDF cells. The results are in line with the ISO specifications of ≥ 70% viability for biomaterials such as dressings [21, 69]. The results confirmed that the films should not cause any skin irritation or present deleterious effect on proliferation of HDFs.

The MTT results of the EGF loaded films are shown in Figure 8. After 24 h, 96% and 97% of the HDF cells were viable in the presence of CH-GE-PEG-EGF and CH-COL-PHARM-PEG-EGF respectively. Compared to corresponding blank 3D printed films (films without EGF), viability of the cells slightly increased after 48 h in CH-GE-PEG-EGF 3D printed films (98%) and for CH-COL-PHARM-PEG-EGF 3D printed films, viability remained the same (97%). From the results in Figure 8, it is evident that both CH-GE-PEG-EGF and CH-COL-PHARM-PEG-EGF 3D printed films were not toxic against HDF cells with cell viability values greater than 70% and will therefore not interfere with cell proliferation. Biomaterials such as COL, CH and EGF are widely used as the main components for fabricating scaffolds for tissue regeneration, while both COL and EGF have important roles in the remodeling and inflammation phases of wound healing along with other biomedical applications owing to their excellent biocompatibility [70].

CH is one of the most commonly natural biopolymers employed for applications such as tissue regeneration, wound healing materials and surgical threads. Moghadas and co-authors [71] and Ahsan and co-authors [72] compared the toxicity profiles of CH films and CH based injectable hydrogels respectively and confirmed the lack of any acute toxic effects of the CH. GE has numerous advantages including biocompatibility, well defined chemistry, and general safety [73]. PHARM is a reference grade of HPMC which is an important polymer in pharmaceutical and food industries being largely used as film forming polymer [74] and therefore generally regarded as safe.

## 4. Conclusions

CH-GE and CH-COL based composite films prepared by 3D printing showed homogenous surface morphology and the presence of PEG/GLY increased flexibility. FTIR results showed specific interactions between CH and GE as well as between CH and COL, PHARM and PEG in the blank films as well as the drug loaded equivalents, indicating that the EGF is also linked with CH through electrostatic interaction. XRD results showed that 3D printed composite CH based films had amorphous properties with all compounds molecularly dispersed in the polymer matrix. *In vitro* adhesion results confirmed the adhesive property of

CH and expected to adhere to the epithelial surface whilst maintaining a moist wound environment. PEG plasticized films exhibited higher swelling capacity than those films containing GLY because PEG allowed increased water ingress. Further, the printed films were able to swell and release the loaded EGF which is useful for managing wound exudate. MTT assay results demonstrated that more than 90% of the cells were viable for all blank 3D printed films after 48 h while approximately 98% and 97% of cells were viable after 48 h for CH-GE-PEG-EGF and CH-COL-PHARM-PEG-EGF 3D printed films respectively. This confirmed that loading of EGF did not affect cell viability but rather slightly enhanced their proliferation. In conclusion, EGF loaded CH-GE-PEG and CH-COL-PHARM-PEG 3D printed films show great potential as promising medicated dressings for chronic wound healing application. However, further studies involving *in vivo* experiments using a mouse model will be required to prove this hypothesis.

**Funding:** "This research did not receive any specific grant from funding agencies in the public, commercial, or not-for-profit sectors".

**Conflicts of Interest:** "The authors declare no conflict of interest."

**Figure Captions**

Figure 1 Tensile profiles (tensile strength, elastic modulus, and percentage elongation at break) for (a) CH-COL-PHARM-PEG films loaded with different plasticizers at different concentrations and (b) EGF loaded 3D printed films showing differences between the two different composite formulations. The results are reported for mean ± standard deviation for three replicates ($n = 3$) and significant differences determined as * = $p < 0.05$; ** = $p \leq 0.01$.

Figure 2 X-ray diffractograms of EGF loaded CH-GE-PEG and CH-COL-PHARM-PEG 3D printed films.

Figure 3 FTIR spectra of EGF loaded (CH-GE-PEG-EGF and CH-COL-PHARM-PEG-EGF) 3D printed films.

Figure 4 SEM images of optimized blank (CH-GE-PEG and CH-COL-PHARM-PEG) and EGF loaded (CH-GE-PEG-EGF and CH-COL-PHARM-PEG-EGF) 3D printed films obtained at a magnification of x500. The images show that all the starting materials (CH, GE, COL, PHARM, PEG and EGF) were homogeneously distributed within the composite 3D

printed film scaffolds, with flat continuous surface indicating that all components achieved good miscibility and compatibility.

Figure 5a Mucoadhesion of plasticized CH-COL-PHARM-PEG films. Data are shown as means ± SD ($n$ = 3). The data were compared by one-way analysis of variance (ANOVA); * represents $p < 0.05$ and ** represents $p \leq 0.01$.

Figure 5b Mucoadhesive results for EGF loaded (CH-GE-PEG-EGF and CH-COL-PHARM-PEG-EGF) 3D printed films ($n$ = 3, ± SD). Data are shown as means ± standard deviation ($n$ = 3). The data were compared by one-way analysis of variance (ANOVA); * represents $p < 0.05$.

Figure 6 Swelling profiles showing the change in the % swelling index with time of (a) blank plasticized CH-COL-PHARM-PEG based films. No significant difference between mean of swelling index of the films 3D printed films was observed; (b) EGF loaded (CH-GE-PEG-EGF and CH-COL-PHARM-PEG-EGF) 3D printed films ($n$ = 3, ± SD).

Figure 7 Drug dissolution profiles showing percentage drug release of EGF with time from CH-GE-PEG-EGF and CH-COL-PHARM-PEG-EGF 3D printed films in PBS at pH 7.4. Data are shown as mean ± SD ($n$ = 4).

Figure 8 Graphical representation of the MTT assay cell viability data (mean ± SD; $n$ = 9) obtained by analyzing HDFs grown in the presence of the CH-GE-PEG-EGF and CH-COL-PHARM-PEG-EGF 3D printed films. Untreated cells and Triton-X −100 were used as negative and positive controls respectively. Data were compared by one-way analysis of variance (ANOVA); * represents $p < 0.05$.

## References


1. J.S. Boateng, O. Catanzano, Advanced therapeutic dressings for effective wound healing-A review, J. Pharm. Sci. 104 (2015) 3653–3680. https:// doi: 10.1002/jps.24610.
2. S. Yun, E. Sim, R. Goh, J. Park, J. Han, Platelet activation: the mechanisms and potential biomarkers. BioMed Res. Int. (2016) 2016, 9060143. DOI: 10.1155/2016/9060143.
3. E.M. Golebiewska, A.W. Poole, Platelet secretion: from haemostasis to wound healing and beyond. Blood Rev. (2015) 29, 153–162. (Doi: 10.1016/j.blre.2014. 10.003).
4. H. Sinno, S. Prakash, Complements and the wound healing cascade: an updated review. Plastic Surg. Int. (2013) 2013, 146764. DOI: 10.1155/2013/146764.
5. O. Catanzano, F. Quaglia, J.S. Boateng, Wound dressings as growth factor delivery platforms for chronic wound healing, Exp. Opin. Drug Del. 18 (2021) 737-759. https://doi: 10.1080/17425247.2021.1867096.
6. S. Cohen, Isolation of a mouse submaxillary gland protein accelerating incisor eruption and eyelid opening in the new-born animal, J. Biol. Chem. 237 (1962) 1555-62. https://doi.org/10.1016/S0021-9258(19)83739-0.
7. R.J. Bodnar, Epidermal growth factor and epidermal growth factor receptor: the Yin and Yang in the treatment of cutaneous wounds and cancer, Adv. Wound Care. 2 (2013) 24–29. doi:10.1089/wound.2011.0326.
8. G. Gainza, S. Villullas, J.L. Pedraz, R.M. Hernandez, M. Igartua. Advances in drug delivery systems (DDSs) to release growth factors for wound healing and skin regeneration, Nanomed. 11 (2015) 1551-1573. doi: 10.1016/j.nano.2015.03.002.
9. N. Khanbanha, F. Atyabi, A. Taheri, F. Talaie, M. Mahbod, R. Dinarvand. Healing efficacy of an EGF impregnated triple gel based wound dressing: in vitro and in vivo studies, BioMed. Res. Int. 493732 (2014) 1-10. https://doi: 10.1155/2014/493732.
10. M. Rodríguez-Vázquez, B. Vega-Ruiz, R. Ramos-Zúñiga, D.A. Saldaña-Koppel, L.F. Quiñones-Olvera. Chitosan and its potential use as a scaffold for tissue engineering in regenerative medicine, Biomed. Res. Int. 2015 (2015) 821279. doi:10.1155/2015/821279.
11. S. Gajbhiye, S. Waikar., Collagen fabricated delivery systems for wound healing: a new roadmap, Biomater. Adv. 142 (2022) 213152. https://doi.org/10.1016/j.bioadv.2022.213152.

12. J. Becerra, M. Rodriguez, D. Leal, K. Norris-Suarez, G. Gonzalez, Chitosan-collagen-hydroxyaptite membranes for tissue engineering. J. Mater. Sci. Mater. Med. 33 (2022) 18. https://doi.org/10.1007/s10856-022-06643-w.
13. C. Holmes, J.S. Wrobel, M.P. MacEachern, B.R. Boles, Collagen-based wound dressings for the treatment of diabetes-related foot ulcers: a systematic review. Diabetes Metab. Syndr. Obes. 6 (2013) 17–29. https://doi:10.2147/DMSO.S36024
14. M. Afzali, J.S. Boateng, Composite fish collagen-hyaluronate based lyophilzed scaffolds modified with sodium alginate for potential treatment of chronic wounds. Polym. 14 (2022) 1550. https://doi: 10.3390/polym14081550.
15. I. Savencu, S. Iurian, A. Porfire, C. Bogdan, I. Tomuta. Review of advances in polymeric wound dressing films. Reactive Func. Polym. 168 (2021) 105059. https://doi.org/10.1016/j.reactfunctpolym.2021.105059.
16. A. Ahmed, J.S. Boateng, Calcium alginate-based antimicrobial film dressings for potential healing of infected foot ulcers. Ther. Del. 9 (2018) 185-204. https://doi: 10.4155/tde-2017-0104.
17. M. Alizadehgiashi, C.R. Nemr, M. Chekini, D.P. Ramos, N. Mittal, S.U. Ahmed, N. Khuu, S.O. Kelley, E. Kumacheva. Multifunctional 3D-Printed Wound Dressings. ACS Nano. 15 (2021) 12375–12387. https://doi:10.1021/acsnano.1c04499.
18. S.V. Kogelenberg, Z. Yue, J.N. Dinoro, C.S. Baker, G.G. Wallace, Three-dimensional printing and cell therapy for wound repair. Adv. Wound Care. 7 (2018) 145-155. https://doi: 10.1089/wound.2017.0752.
19. F. Hafezi, N. Scoutaris, D. Douroumis, J. Boateng, 3D printed chitosan dressing crosslinked with genipin for potential healing. Int. J. Pharm. 560, (2019) 406–415. https://doi:10.1016/j.ijpharm.2019.02.020.
20. O.C. Okeke, J.S. Boateng, Nicotine stabilisation in composite sodium alginate based wafers and films for nicotine replacement therapy. Carbohydr. Polym. 155 (2017) 78-88. https://doi.org/10.1016/j.carbpol.2016.08.053.
21. A. Ahmed, G.T.M. Getti, J.S. Boateng, Medicated multi-targeted alginate-based dressings for potential treatment of mixed bacterial-fungal infections in diabetic foot ulcers. Int. J. Pharm. 606 (2021) 120903-120920. https://doi:10.1016/j.ijpharm.2021.120903.
22. J.S. Boateng, I. Ayensu, Preparation and characerisation of laminated thiolated chitosan-based freeze-dried wafers for potential buccal delivery of macromolecules.

Drug Dev. Ind. Pharm. 40 (2014) 611-618. https://doi:10.3109/03639045.2014.884126

23. E. Szymańska, K. Winnicka, Stability of chitosan-A challenge for pharmaceutical and biomedical applications. Mar. Drugs. 13 (2015) 1819-1846. https://doi: 10.3390/md13041819.
24. N. Scoutaris, A. A. Nion, Hurt, D. Douroumis, Jet dispensing as a high throughput method for rapid screening and manufacturing of cocrystals. Cryst. Eng. Comm. 18 (2016) 5079–5082. https://doi.org/10.1039/C6CE00664G.
25. D. Mukherjee, S. Bharath, Design and characterization of double layered mucoadhesive system containing bisphosphonate derivative. ISRN Pharm. 2013(604690), (2013) 1-7. https://doi: 10.1155/2013/604690.
26. Y. Takeuchi, N. Ikeda, K. Tahara, H. Takeuchi. Mechanical characteristics of orally disintegrating films: comparison of folding endurance and tensile properties. Int. J. Pharm. 589 (2020) 119876. https://doi.org/10.1016/j.ijpharm.2020.119876

27. G. Khan, S.K. Yadav, R.R. Patel, Development and evaluation of biodegradable chitosan films of metronidazole and levofloxacin for the management of periodontitis. AAPS PharmSciTech. 17 (2016) 1312-1325. https://doi:10.1208/s12249-015-0466-y.
28. J.S.D. Petroudy, Advanced High Strength Natural Fibre Composites in Construction, first ed., Woodhead Publishing, Sawston, Cambridge, 2016. pp. 59-83.
29. F. Momoh, J.S. Boateng, S.C.W. Richardson, B.Z. Chowdhry, J.S. Mitchell. Development and functional characterization of alginate dressing as potential protein delivery system for wound healing. Int. J. Biol. Macromol. 81, (2015). 137-150. https://doi.org/10.1016/j.ijbiomac.2015.07.037
30. G. Kaur, D. Singh, V. Brar, Bioadhesive okra polymer based buccal patches as platform for controlled drug delivery. Int. J. Biol. Macromol. 2014, 70 408–419. https://doi:10.1016/j.ijbiomac.2014.07.015.
31. T. Karbowiak, H.Hervet, L. Léger, D. Champion, F. Debeaufort, A. Voilley, Effect of plasticizers (water and glycerol) on the diffusion of a small molecule in Iota-carrageenan biopolymer films for edible coating application. Biomacromol. 7 (2006) 2011–2019. https://doi:10.1021/bm060179r.
32. J.S. Boateng, H. Pawar, J. Tetteh, Polyox and carrageenan based composite film dressing containing antimicrobial and antiinflammatory drugs for effective wound

healing. Int. J. Pharm. 441 (2013) 181-191. https://doi.org/10.1016/j.ijpharm.2012.11.045.

33. D.R. Tapia-Blácido, P. Sobral, F.C. Menegalli, Effect of drying conditions and plasticizer type on some physical and mechanical properties of amaranth flour films. LWT Food Sci. Technol. 50 (2013) 392–400. https://doi.org/10.1016/j.lwt.2012.09.008.
34. J.P. Hong, H.D. Jung, Y.W. Kim, Recombinant human epidermal growth factor (EGF) to enhance healing for diabetic foot ulcers. Ann. Plast. Surg. 56 (2006) 394-400. https://doi:10.1097/01.sap.0000198731.12407.0c.
35. I. Leceta, P. Guerrero, I. Ibarburu, M.T. Dueñas, Characterization and antimicrobial analysis of chitosan-based films. J. Food Eng. 116 (2013) 889–899. https://doi.org/10.1016/j.jfoodeng.2013.01.022.
36. M. Liu, Y. Zhou, Y. Zhang, C. Yu, S. Cao, Preparation and structural analysis of chitosan films with and without sorbitol. Food Hydrocoll. 33 (2013) 186-191. https://doi.org/10.1016/j.foodhyd.2013.03.003.
37. H.S. Lu, J.J. Chai, M. Li, B.R. Huang, Crystal structure of human epidermal growth factor and its dimerization. The J. Biol. Chem. 276 (2001) 34913-34917. https://doi.org/10.1074/jbc.M102874200.
38. X. Lu, H. Zhang, Y. Huang, Y. Zhang, A proteomics study to explore the role of adsorbed serum proteins for PC12 cell adhesion and growth on chitosan and collagen/chitosan surfaces. Regen. Biomater. 5 (2018) 261–273. https://doi:10.1093/rb/rby017
39. X.Y. Wang, G. Wang, L. Liu, The mechanism of a chitosan-collagen composite film used as biomaterial support for MC3T3-E1 cell differentiation. Sci. Reports 6 (2016) 1-8. https://doi:10.1038/srep39322.
40. P. Kolhe, R.M. Kannan, Improvement in ductility of chitosan through blending and copolymerization with PEG: FTIR investigation of molecular interactions. Biomacromol. 4 (2003) 173-80. https://doi.org/10.1021/bm025689+.
41. L.L. Fernandes, C.X. Resende, D.S. Tavares, Soares, G.A. Cytocompatibility of chitosan and collagen-chitosan scaffolds for tissue engineering. Polímeros, 21 (2011) 1-6. http://dx.doi.org/10.1590/S0104-14282011005000008.
42. M. Rajama, S. Pulavendrana, C. Rosea, A.B. Mandal, Chitosan nanoparticles as a dual growth factor delivery system for tissue engineering applications. Int. J. Pharm. 410 (2011) 145-152. https://doi.org/10.1016/j.ijpharm.2011.02.065.

780 43. Y. Dong, Y. Li, Z. Ma, Z. Rao, X. Zheng, K. Tang, J. Liu. Effect of polyol
781 plasticizers on properties and microstructure of soluble soybean polysaccharide edible
782 films. Food Packag. Shelf Life. 35 (2023) 101023.
783 https://doi.org/10.1016/j.fpsl.2022.101023.
784 44. A.A.B.A. Mohammed, Z. Hasan, A.A.B. Omran, A.M. Elfaghi, M.A. Khattak, R.A.
785 Ilyas, S.M. Sapuan, Effect of various plasticizers in different concentrations on
786 physical, thermal, mechanical and structural properties of wheat starch-based films.
787 Polym. 15 (2023) 63. https://doi.org/10.3390/polym15010063 .
788 45. J. Tarique, S.M. Sapuan, A. Khalina, Effect of glycerol plasticizer loading on the
789 physical, mechanical, thermal and barrier propertes of arrowroot (Maranta
790 arundinacea) starch biopolymers. Scientific Reports. 11 (2021) 13900.
791 https://doi.org/10.1038/s41598-021-93094-y.
792 46. M. Vieira, M.A. da Silva, L.O. dos Santos, M.M. Beppu, Natural-based plasticizers
793 and biopolymer films: A review. Eur. Polym. J. 47 (2011) 254-263.
794 https://doi.org/10.1016/j.eurpolymj.2010.12.011.
795 47. A. Sionkowska, B. Kaczmarek, J. Stalinska, A.M. Osyczka, Biological properties of
796 chitosan/collagen composites. Key Eng. Mater. 587 (2014) 205-210.
797 https://doi.org/10.4028/www.scientific.net/KEM.587.205.
798 48. A. Sionkowska, B. Kaczmarek, R. Gadzala-Kopciuch, Gentamicin release from
799 chitosan and collagen composites. J. Drug Del. Sci. Technol. 35 (2016) 353-359.
800 https://doi.org/10.1016/j.jddst.2016.09.001.
801 49. A. Faikrua, R. Jeenapongsa, M. Sila-asna, J. Viyoch, Properties of b-glycerol
802 phosphate/collagen/chitosan blend scaffolds for application in skin tissue engineering.
803 Sci. Asia 35 (2009) 247-254. https://doi:10.2306/SCIENCEASIA1513-
804 1874.2009.35.247.
805 50. V. Yadav, A. Gupta, J.S. Yadav, B. Kumar, Mucoadhesive polymers: Means of
806 improving the mucoadhesive properties of drug delivery system. J. Chem. Pharm.
807 Res. 2 (2010) 418-432. https://doi:10.4103/0975-7406.76478.
808 51. T. Yu, G.P. Andrews, D.S. Jones, 2014. Mucosal Delivery of Biopharmaceuticals., in:
809 J.D. Neves, B. Sarmento (Eds) Mucoadhesion and Characterization. Boston, MA:
810 Springer, pp. 35-58. https://doi:10.1007/978-1-4614-9524-6_2.
811 52. D.R. Tapia-Blácido, P. Sobral, F.C. Menegalli, Effect of drying conditions and
812 plasticizer type on some physical and mechanical properties of amaranth flour films.

LWT Food Sci. Technol. 50 (2013) 392–400. https://doi.org/10.1016/j.lwt.2012.09.008.

53. S. Razavi, A.M. Amini, Y. Zahedi, Characterisation of a new biodegradable edible film based on sage seed gum: Influence of plasticiser type and concentration, Food Hydrocoll. 43 (2015) 290–298. https://doi.org/10.1016/j.foodhyd.2014.05.028.
54. D. Muscat, B. Adhikari, R. Adhikari, D.S. Chaudhary, Comparative study of film forming behaviour of low and high amylose starches using glycerol and xylitol as plasticizers. J. Food Eng. 109 (2012) 189–201. https://doi.org/10.1016/j.jfoodeng.2011.10.019.
55. S.K. Ramineni, C.B. Fowler, P.D. Fisher, L.L. Cunningham Jr, D.A. Puleo, Effects of epidermal growth factor-loaded mucoadhesive films on wounded oral tissue rafts. Biomed. Mater. 10 (2015) 015026. https://doi:10.1088/1748-6041/10/1/015026
56. R.A. Bader, D.A. Putnam, (Eds). Engineering Polymer Systems for Improved Drug Delivery. John Wiley & Sons, Inc. 2013.
57. D.W. Lee, C. Lim, J.N. Israelachvili, D.S. Hwang, Strong adhesion and cohesion of chitosan in aqueous solutions. Langmuir, 29 (2013) 14222–14229. https://doi:10.1021/la403124u.
58. M. Zhang, X.H. Li, Y.D. Gong, N.M. Zhao, X.F. Zhang, Properties and biocompatibility of chitosan films modified by blending with PEG. Biomater. 23 (2002) 2641-2648. https://doi.org/10.1016/S0142-9612(01)00403-3.
59. R.A. Siegel, M.J. Rathbone, Overview of controlled release mechanisms. in: J. Siepmann, R.A. Siegel, M.J. Rathbone (eds). Fundamentals and applications of controlled release drug delivery. Springer, Minneapolis, 2012, pp. 19-43. https://doi: 10.1007/978-1-4614-0881-9_2
60. S.K. Roy, B. Prabhakar, Bioadhesive polymeric platforms for transmucosal drug delivery systems - A review. Tropic. J. Pharm. Res. 9 (2010) 91-104. https://doi: 10.4314/tjpr.v9i1.52043.
61. J.R. Khurma, A.V. Nand, Temperature and pH sensitive hydrogels composed of chitosan and poly(ethylene glycol). Polym. Bullet. 59 (2008) 805–812. https://doi.org/10.1007/s00289-007-0817-2.
62. E. Budianto, S. Prilia, M.N. Mardhat, Effect of crosslinking agents, pH and temperature on swelling behavior of swelling behavior of cross-linked chitosan hydrogel. Asian J. Appl. Sci. 3 (2015) 581-588. https://www.ajouronline.com/index.php/AJAS/article/view/3099.

63. H. Cassimjee, P. Kumar, P. Ubanako, Y.E. Choonara, Genipin-crosslinked polysaccharide scaffolds for potential neural tissue engineering applications. Pharmaceutics. 14 (2022) 441. doi:10.3390/pharmaceutics14020441.
64. C. Alemdaroglu, Z. Degim, F. Zor, S. Ozturk, D. Erdogan, An investigation on burn wound healing in rats with chitosan gel formulation containing epidermal growth factor. Burns, 32 (2006) 319–327. https://doi:10.1016/j.burns.2005.10.015.
65. P. Koria, Delivery of growth factors for tissue regeneration and wound healing. BioDrugs. 26 (2012) 163–175. https://doi:10.2165/11631850-000000000-00000.
66. J.W. Park, S.R. Hwang, I.-S. Yoon, Advanced growth factor delivery systems in wound management and skin regeneration. Mol. 22 (2017) 1259. https://doi:10.3390/molecules22081259
67. National Institute of Clinical Excellence (NICE) Guidance. Evidence Summary (ESMPB2). Chronic wounds: advanced wound dressings and antimicrobial dressings (30 March 2016). https://www.nice.org.uk/advice/esmpb2/chapter/key-points-from-the-evidence Available at (accessed 03 June, 2023)
68. O. Catanzano, R. Docking, P.A. Schofield, J.S. Boateng, Advanced multi-targeted composite biomaterial dressing for pain and infection control in chronic leg ulcers. Carbohydr. Polym. 172 (2017) 40-48. https://doi.org/10.1016/j.carbpol.2017.05.040.
69. S. Moritz, C. Wiegand, F. Wesarg, N. Hessler, F.A. Muller, D. Kralisch, U-C. Hipler, D. Fischer, Active wound dressings based on bacterial nanocellulose as drug delivery system for octenidine. Int. J. Pharm. 471 (2014) 45-55. https://doi.org/10.1016/j.ijpharm.2014.04.062.
70. V. Patrulea, V. Ostaf, G. Borchard, O. Jordan, Chitosan as a starting material for wound healing. Eur. J. Pharm. Biopharm. 97 (2015) 417-26. https://doi.org/10.1016/j.ejpb.2015.08.004.
71. B. Moghadas, E. Dashtimoghadam, H. Mirzadeh, F. Seidi, M.M. Hasani-Sadrabadi, Novel chitosan-based nanobiohybrid membranes for wound dressing applications. RSC Adv. 6 (2016) 7701–7711.https://doi.org/10.1039/C5RA23875G.
72. A. Ahsan, M.A. Farooq, A. Parveen, Thermosensitive chitosan based injectable hydrogel as an efficient anticancer drug carrier. ACS Omega. 5 (2020) 820450-20460. https://doi.org/10.1021/acsomega.0c02548.
73. W. Winotapun, P. Opanasopit, T. Ngawhirunpat, T. Rojanarata, One-enzyme catalyzed simultaneous plant cell disruption and conversion of released glycoside to aglycone combined with in situ product separation as green one-pot production of

genipin from gardenia fruit. Enzyme Microb. Technol. 53 (2013) 92-96. https://doi.org/10.1016/j.enzmictec.2013.05.001.

74. G. Perfetti, T. Alphazan, P. van Hee, W.J. Wilderboer, G.M. Meesters, Relation between surface roughness of free films and process parameters in spray coating. Eur J. Pharm. Sci. 42 (2011) 262-272. DOI:10.1016/j.ejps.2010.12.001.

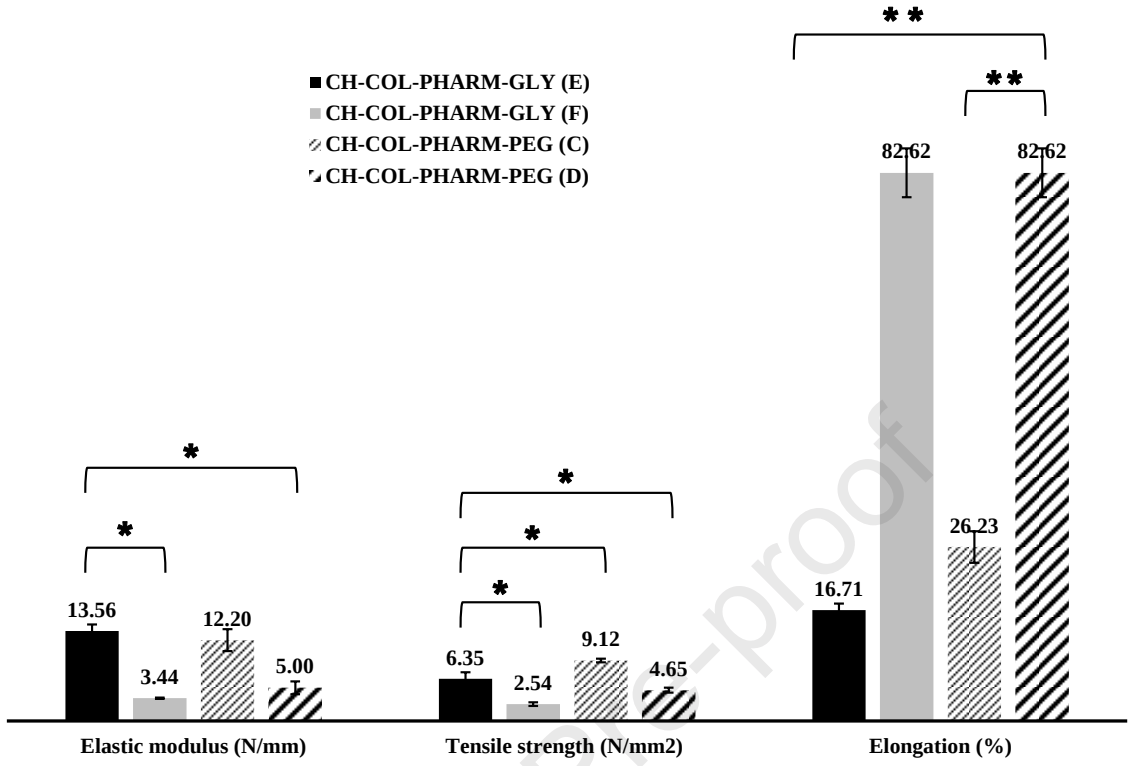


(a)

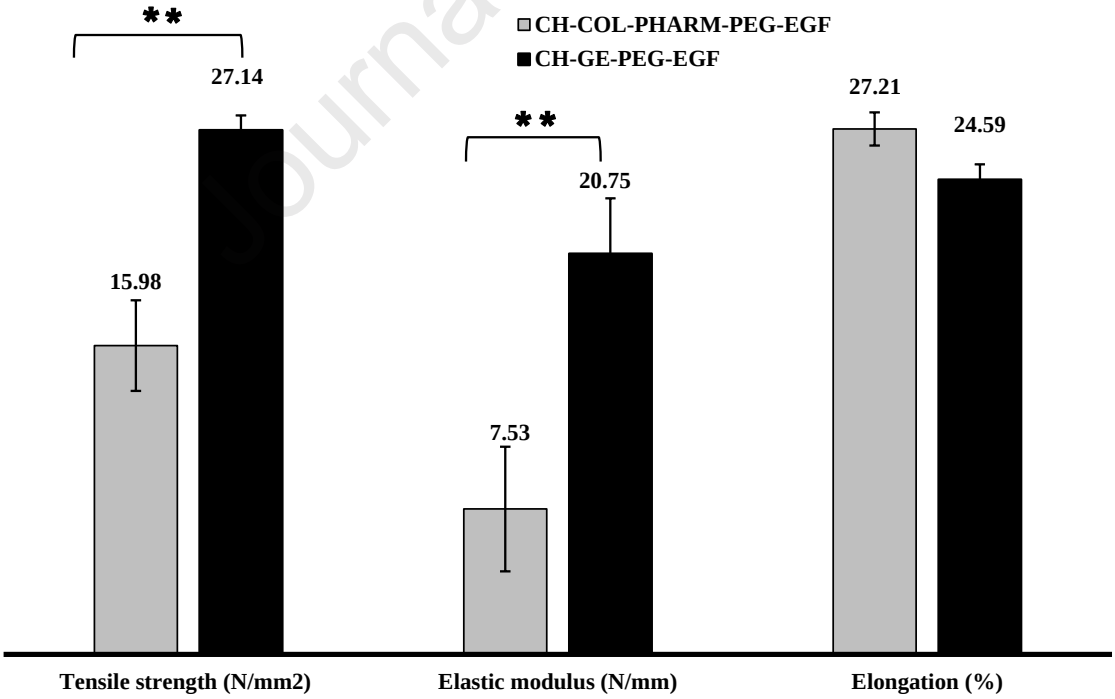


(b)

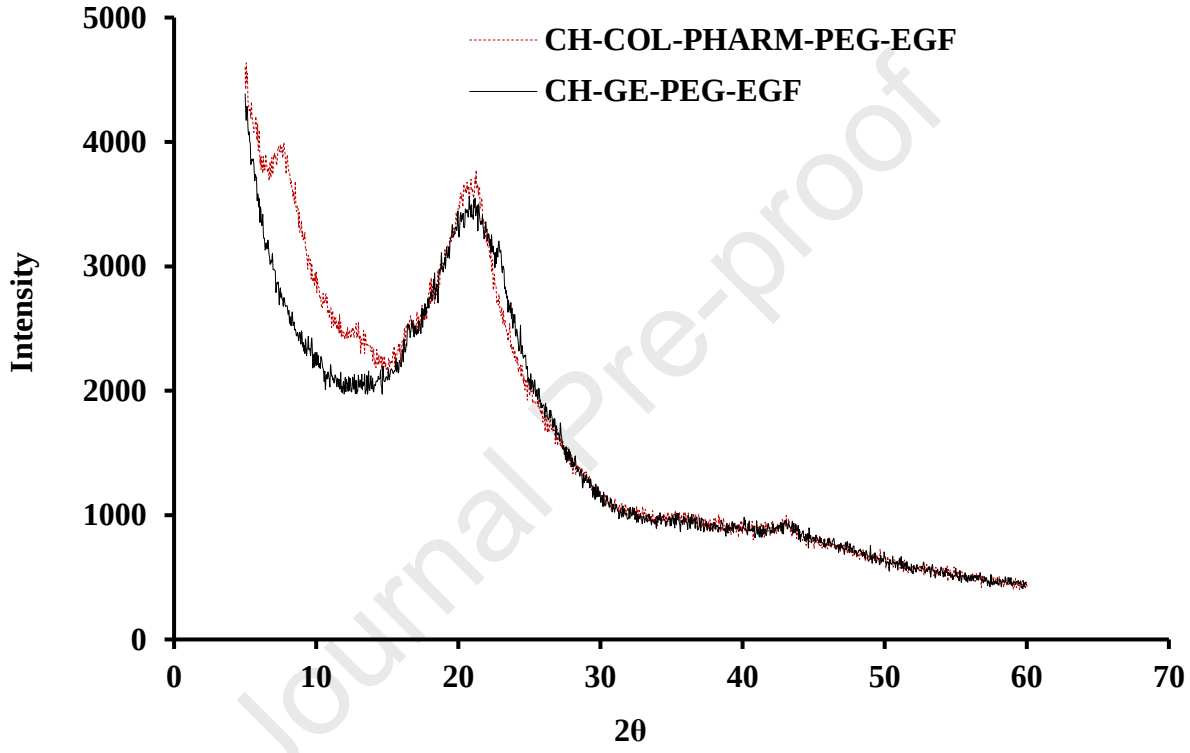

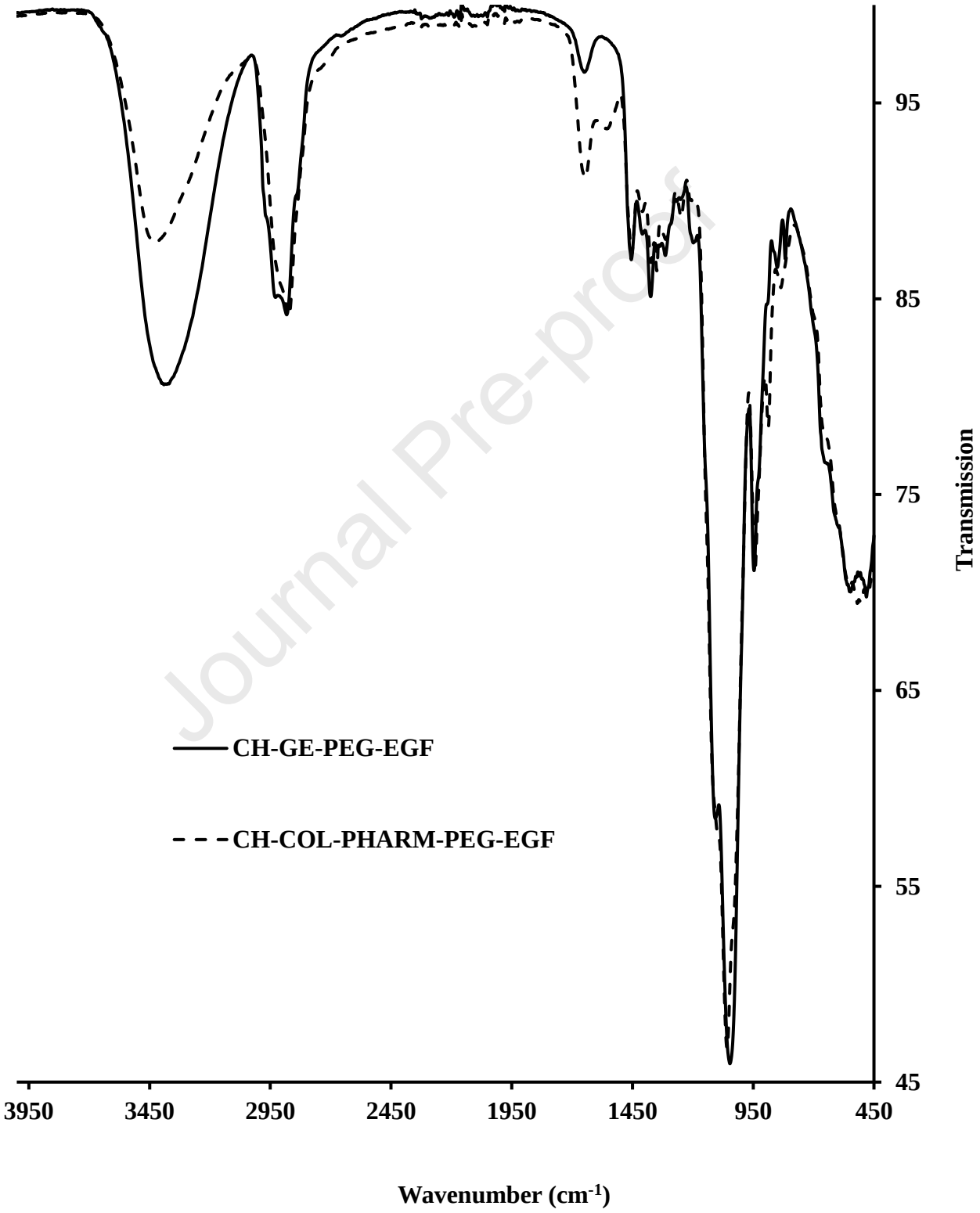

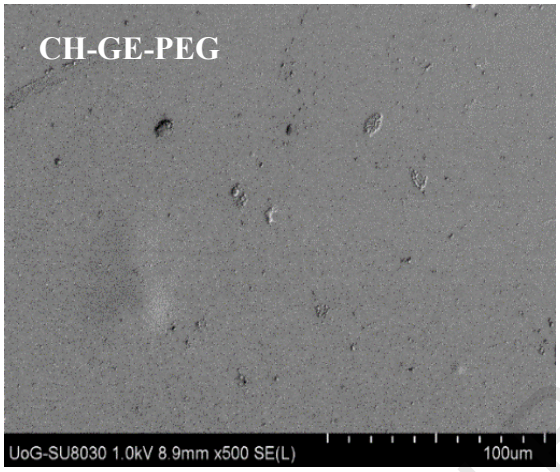
CH-GE-PEG
UoG-SU8030 1.0kV 8.9mm x500 SE(L)
100um

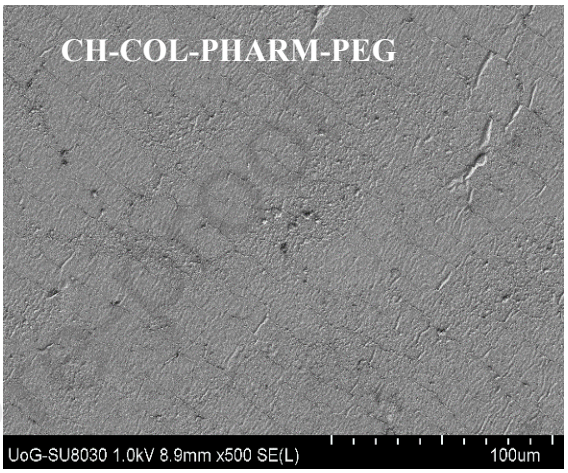
CH-COL-PHARM-PEG
UoG-SU8030 1.0kV 8.9mm x500 SE(L)
100um

(a)

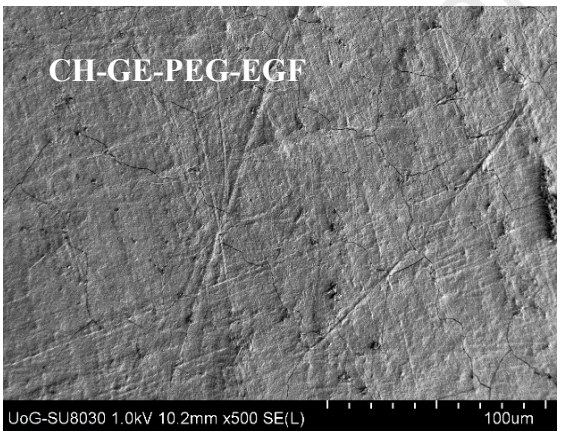
CH-GE-PEG-EGF
UoG-SU8030 1.0kV 10.2mm x500 SE(L)
100um

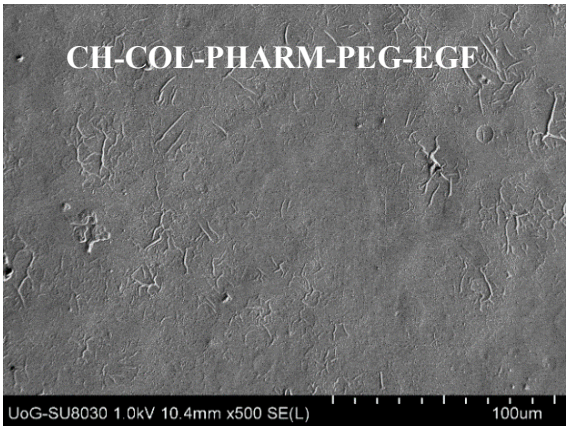
CH-COL-PHARM-PEG-EGF
UoG-SU8030 1.0kV 10.4mm x500 SE(L)
100um

(b)

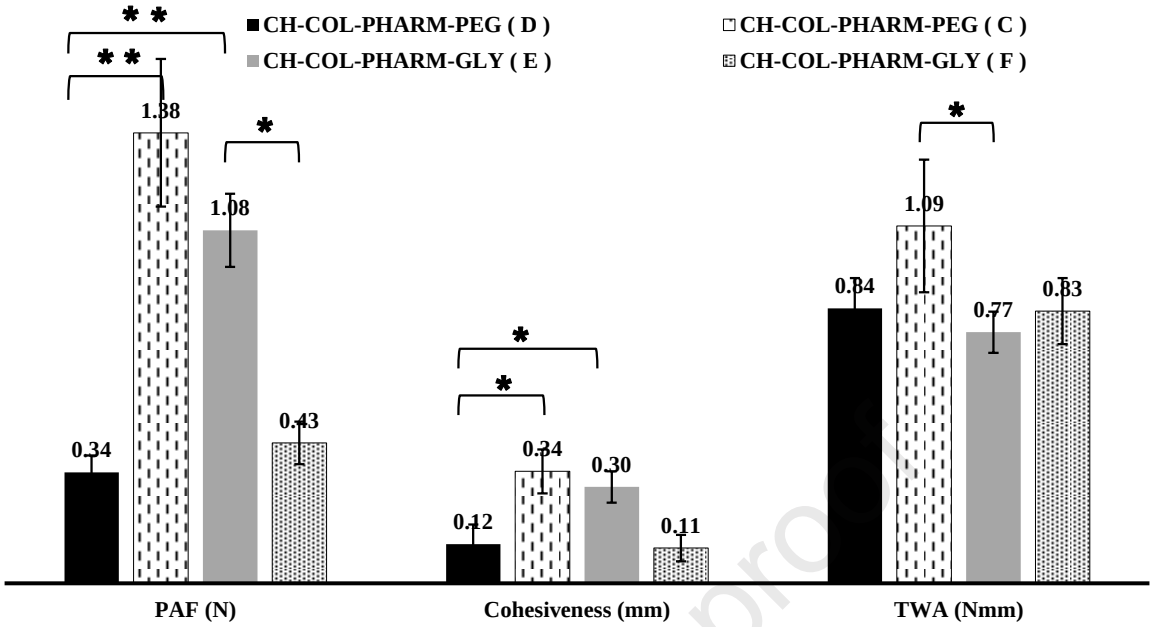


(a)

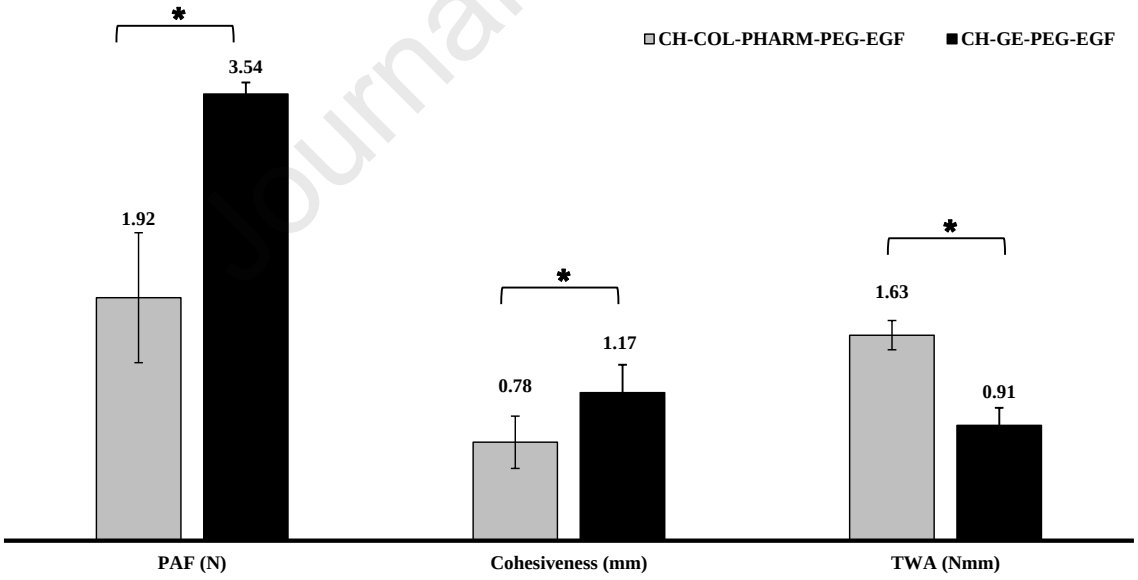


(b)

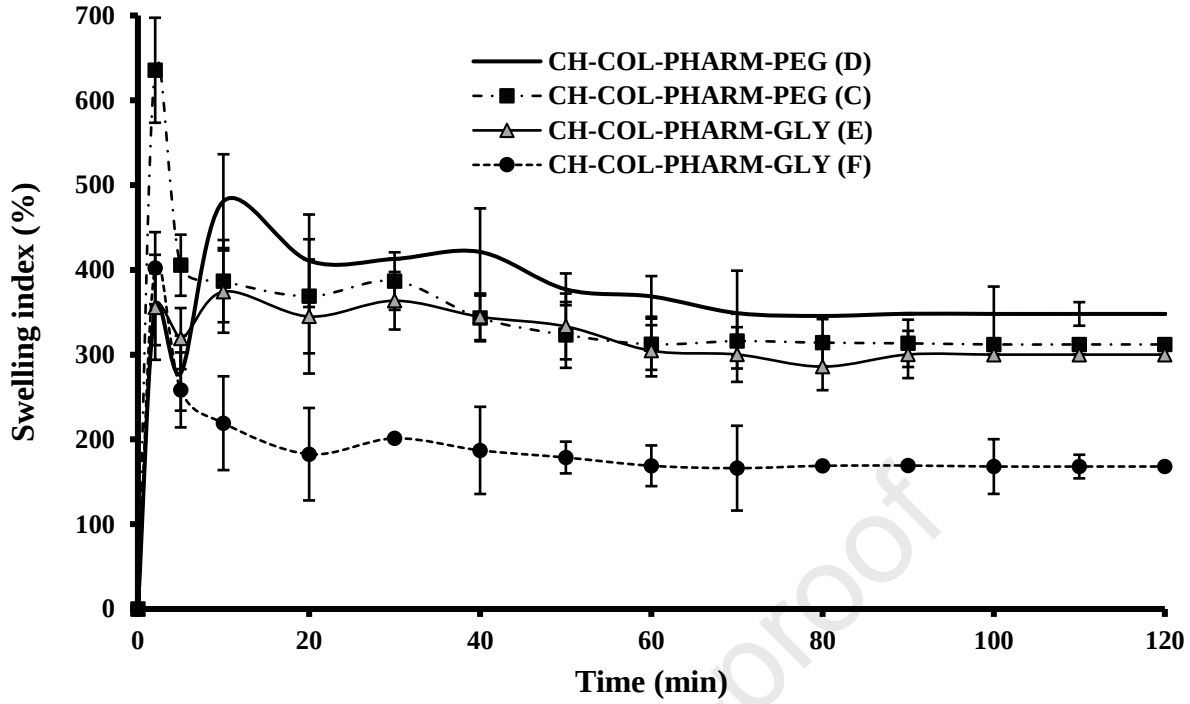


(a)

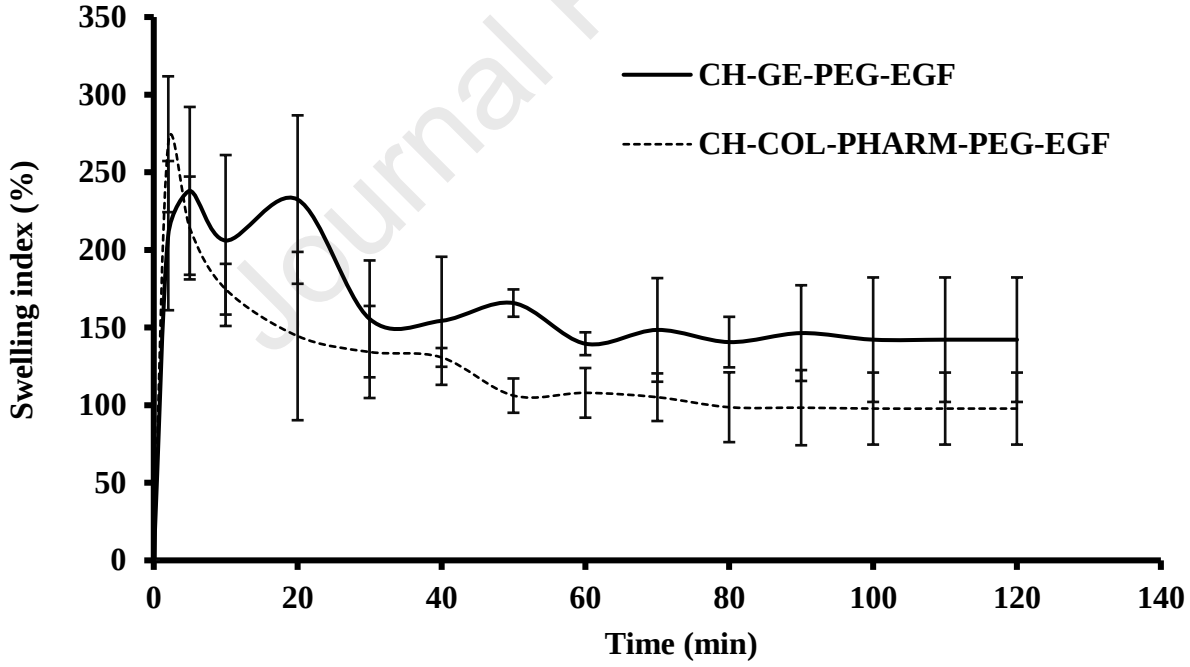


(b)

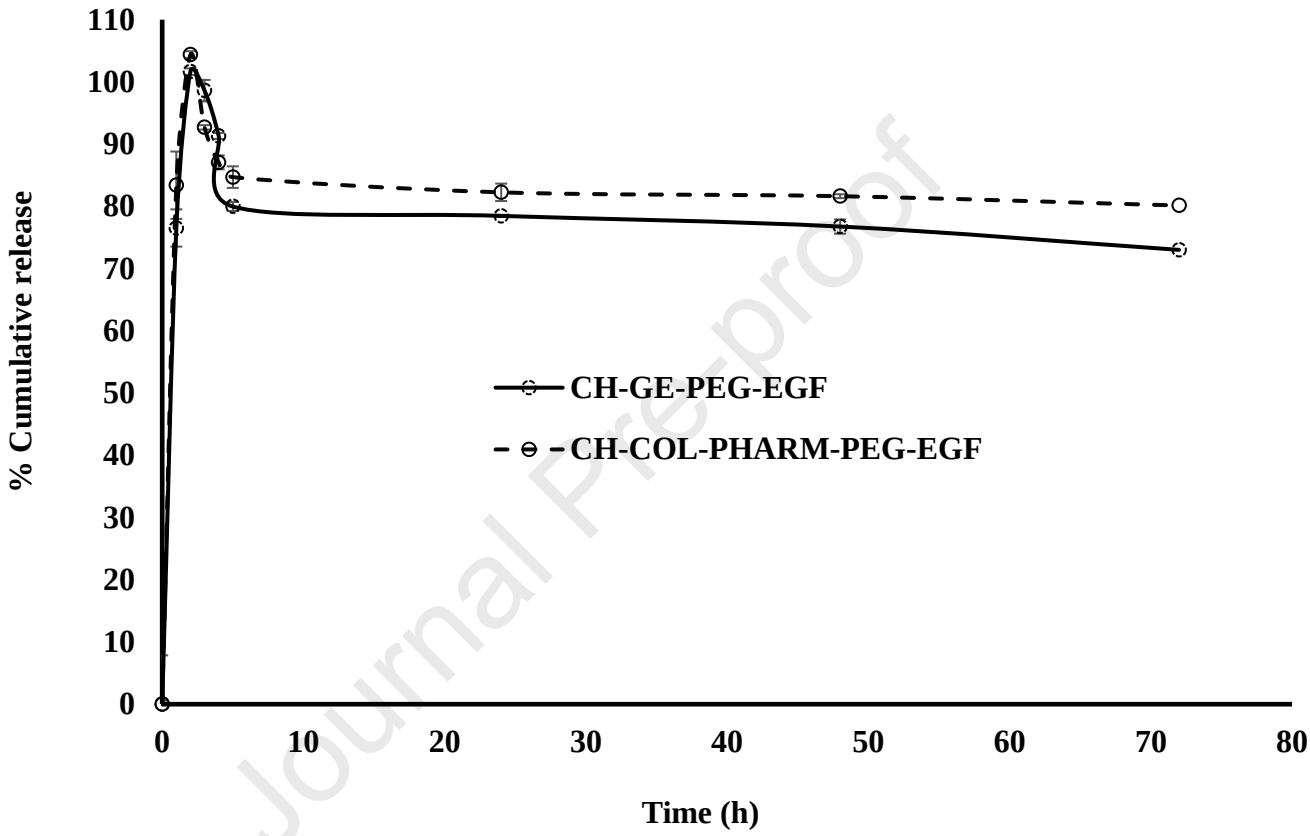

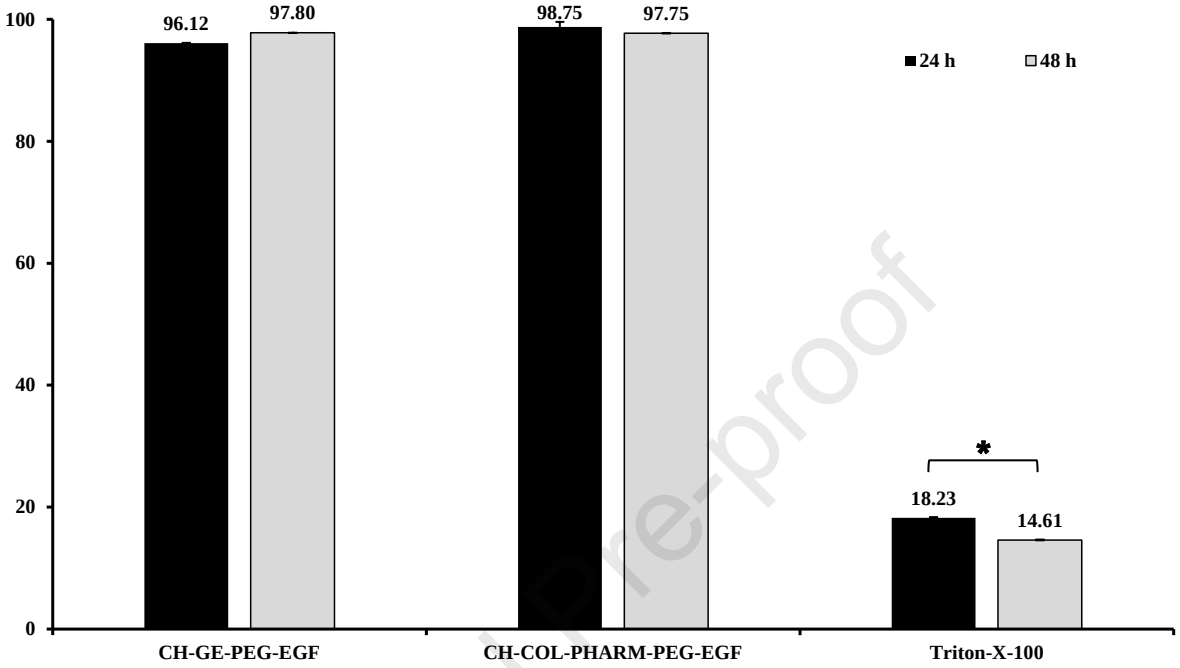

**Author Contributions:**

"Conceptualization: JSB & DD; methodology: FH & AGT; software: DD; validation: JSB, DD, FH, &AGT; formal analysis: FH; investigation: FH & AGT; resources: JSB & DD; data curation: FH; writing – preparation of original draft: JSB; writing - review and editing: FH, AGT & DD; visualization: FH; supervision: JSB & DD; project administration: JSB; funding acquisition: JSB & DD. All authors have read and agreed to the published version of the manuscript. (JSB: Joshua Siaw Boateng; FH: Forough Hafezi; AGT: Atabak Ghanizadeh Tabriz; DD: Dennis Douroumis)

## Declaration of Interest Statement

The authors declare no conflicts of interest